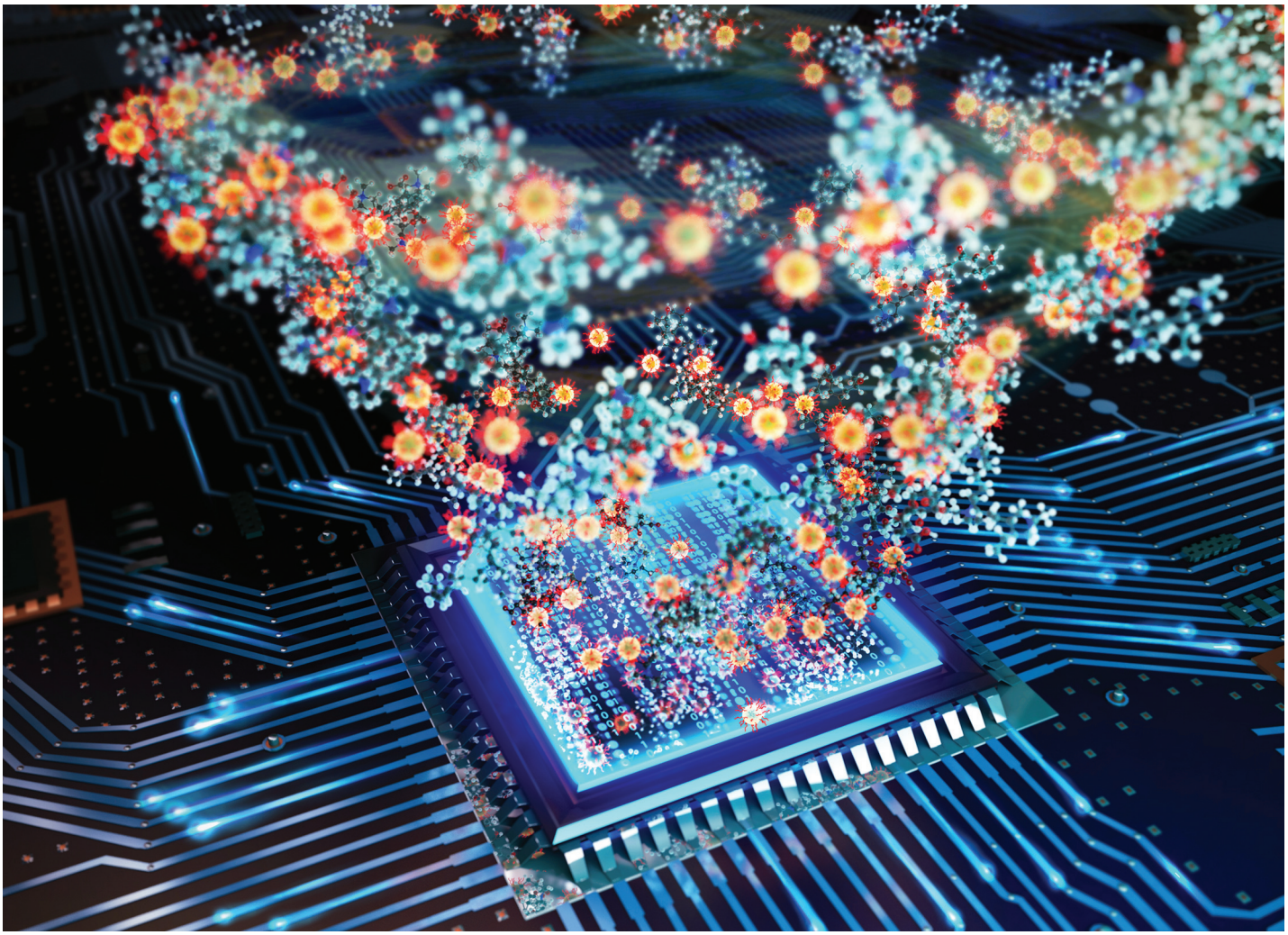

Showcasing work from the Nano Materials and Functional Ultrathin Film Laboratory, Department of Chemical & Biological Engineering, Korea University, Seoul, Republic of Korea.

Functional nanocomposites with perfect nanoblending between water-soluble polymers and hydrophobic inorganic nanoparticles: applications to electric-stimuli-responsive films

We introduce hydrophilic/hydrophobic layer-by-layer (H/H LbL) assembly allowing perfect nanoblending between water-soluble polymers and hydrophobic NPs. Unipolar switching nonvolatile memory devices prepared with H/H LbL assembly gave excellent memory performances with a high ON/OFF current ratio of ~109 and a low OFF current of ~10–12 A. Furthermore, our approach is applicable to the design of various biocompatible nanocomposite films and electrochemical devices.

As featured in:

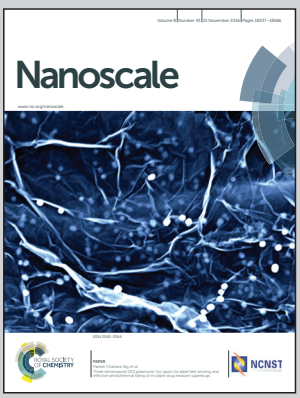

See Jai-Kyeong Kim, Jinhan Cho *et al.*, *Nanoscale*, 2016, **8**, 18315.

ROYAL SOCIETY OF CHEMISTRY

www.rsc.org/nanoscale

Registered charity number: 207890

Nanoscale

PAPER

View Article Online
View Journal | View Issue

Cite this: *Nanoscale*, 2016, **8**, 18315

Functional nanocomposites with perfect nanoblending between water-soluble polymers and hydrophobic inorganic nanoparticles: applications to electric-stimuli-responsive films†

Sanghyuk Cheong,[a] Jai-Kyeong Kim*[b] and Jinhan Cho*[a]

Received 22nd June 2016,
Accepted 1st September 2016

DOI: 10.1039/c6nr05007g

www.rsc.org/nanoscale

There is rising demand for metal or metal oxide nanoparticle (NP)/polymer nanocomposite films with desired functionalities. However, it is difficult to directly combine well-defined NPs synthesized using organic fatty acids in nonpolar media with water-soluble polymers, except polyelectrolytes with specific functional moieties, because they differ in their hydrophobic/hydrophilic properties. We have developed a facile and universal hydrophilic/hydrophobic layer-by-layer (LbL) assembly method that enables perfect nanoblending between water-soluble polymers and hydrophobic NPs, maintaining their specific functionalities. Various hydrophobic NPs stabilized by using oleic acid (OA) (*e.g.*, OA-TiO_2, OA-Fe_3O_4, OA-Ag, and OA-Pt NPs) were directly LbL assembled with various water-soluble polymers (including biomaterials) containing carboxylic acid (–COOH), tertiary ammonium (N^+), hydroxyl (–OH), and/or ether (–O–) groups. This adsorption behavior is based on the affinities between water-soluble polymers with multidentate binding sites and the surfaces of metal or metal oxide NPs stabilized by OA ligands. Our approach can be used to fabricate unipolar switching nonvolatile memory devices with ON/OFF current ratios greater than ~10^{10} and good memory stability, despite the use of water-soluble polymers.

1. Introduction

Polymer/inorganic nanoparticle (NP) nanocomposite films, which can be prepared by mixture blending,[1] self-assembly of block copolymers,[2,3] molecular recognition,[4,5] Langmuir–Blodgett methods,[6] coordination-driven assembly,[7] or layer-by-layer (LbL) assembly,[8–22] have been widely investigated in various potential applications ranging from biological films to nonvolatile memory devices for data-storage systems in mobile electronics. Much attention has been focused on nanocomposite films with the expectation that specific combinations of functional polymers and inorganic NPs could enable the development of nanocomposite film devices with desired performances and lead to the development of novel functional materials/films that do not require complicated chemical syntheses.[5–23]

Inorganic NPs of uniform size and high crystallinity can be synthesized using hydrophobic ligands in nonpolar media rather than in aqueous media.[24,25] Hydrophobic ligands such as organic fatty acids, *e.g.*, oleic acid (OA) or palmitic acid, in particular, have been widely used to synthesize well-defined inorganic NPs, including metals and metal oxides. However, despite their advantages, the hydrophobic properties of organic fatty acid ligands have limitations in terms of direct combination with hydrophobic polymers without the use of additional polymer binders because thermodynamically unfavorable interfacial interactions between polymers and inorganic NPs may cause serious large-scale NP agglomeration or segregation.[26] Direct and perfect combination of hydrophobic inorganic NPs and functional water-soluble polymers with differing hydrophobic/hydrophilic properties has not yet been achieved. These problems have restricted the preparation of NP/polymer nanocomposite-based assemblies that require a high level of control over the loading amounts, thicknesses, and uniform dispersions of NPs and polymers.

Among the many nanocomposite film preparation methods, LbL assembly, which involves the successive adsorption of components through complementary interactions between neighboring components in the same solvent (generally aqueous/aqueous or organic/organic media), is the most versatile and enables the preparation of functional nano-

[a]*Department of Chemical and Biological Engineering, Korea University, Anam-dong, Seongbuk-gu, Seoul 136-713, Republic of Korea. E-mail: jinhan71@korea.ac.kr*
[b]*Photoelectronic Hybrid Research Center, Korea Institute of Science and Technology, Hwarang-ro 14-gil, Seongbuk-gu, Seoul 136-791, Republic of Korea. E-mail: jack@kist.re.kr*

†Electronic supplementary information (ESI) available. See DOI: 10.1039/c6nr05007g

composite films with precisely controlled thicknesses and chemical compositions.[8–22] Recent advances in the LbL assembly of hydrophobic NPs and polymers have been based on the use of neutral amine (NH_2)-induced nucleophilic substitution,[19,22] and NH_2-induced ligand-exchange reactions[17,20] in organic/organic solvent systems without the aid of a phase-transfer process or nanocontainers such as block copolymer micelles. Such nanocomposite films have also been shown to be applicable to the preparation of energy-harvesting/storage devices,[17] catalytic colloids,[27] and bipolar switching nonvolatile memory devices (*i.e.*, devices with voltage-polarity-dependent resistance changes)[22] with high ON/OFF current ratios of $\sim 10^3$.

Our group recently reported a strong-electrolyte-induced amphiphilic LbL assembly method that enabled the assembly of OA-NPs in toluene with a strong polyelectrolyte (PE) [*i.e.*, poly(styrenesulfonic acid) (PSS)] or graphene oxide functionalized with SO_3^- groups in aqueous media.[28] We also showed that these LbL-assembled films can be used in supercapacitor electrodes, which require good electrical and/or ionic conductivity, because the strong sulfonic acid groups of PSS can promote electrochemical oxidation (*i.e.*, an increase in the current density) of multilayer films. However, such an approach is unsuitable for the fabrication of data-storage films, which need a low leakage current level. Furthermore, although our previous approach led to the first successful combination of the advantages of a strong-PE-based electrostatic LbL assembly in aqueous media and covalent LbL assembly in nonpolar media, it has not been extended to water-soluble (charged and uncharged) polymers containing carboxylate ions ($-COO^-$), tertiary ammonium (N^+), hydroxyl (–OH), ether (–O–), and/or amino acid groups. Our method is therefore still restricted in terms of material selection because the bridging organic components for the LbL assembly of hydrophobic NPs (mainly OA-NPs) are limited to NH_2-functionalized polymers in an organic solvent or SO_3^--functionalized PEs in aqueous media. The type of inserted polymer and the type of NP both substantially affect the uses, functionalities, and performances of LbL-assembled NP films.[28–32] The development of versatile and direct LbL assemblies of well-defined hydrophobic metal (or metal oxide) NPs and various water-soluble polymers, giving complete fusion between hydrophobic NPs and hydrophilic polymers in nanocomposite films, is therefore a challenge.

In this study, we developed a facile and versatile hydrophilic/hydrophobic (H/H) LbL assembly, which enables perfect nanoblending between hydrophobic metal (or metal oxide) NPs stabilized by OA ligands, *i.e.*, OA-Ag, OA-Pt, OA-TiO_2, and OA-Fe_3O_4 NPs, in nonpolar media and water-soluble polymers, *i.e.*, anionic poly(acrylic acid) (PAA) with carboxylate ions, cationic poly(diallyldimethylammonium chloride) (PDDA) with tertiary ammonium groups, poly(vinyl alcohol) (PVA) with hydroxyl groups, poly(ethylene oxide) (PEO) with ether groups, and biomaterials, *i.e.*, catalase (CAT), ferritin, and hemoglobin, with numerous amino acid residues, in aqueous media. Our approach is based on the fact that hydrophobic OA ligands bound to inorganic NP surfaces are easily replaced by a variety of multibinding site groups (*i.e.*, hydrophilic groups) of water-soluble polymers during the build-up of multilayers. In the cases of weak PEs such as PAA, in particular, the adsorbed amount (or packing density) of hydrophobic NPs can be easily adjusted *via* the pH and concentration of the weak PE solution. This behavior is almost identical to the adsorption behavior in a traditional weak-PE-based electrostatic LbL assembly. These phenomena imply that numerous hydrophobic NPs can be completely combined with almost all water-soluble polymers without any NP segregation or aggregation.

We showed that our approach based on H/H LbL assembly adsorption properties can be effectively applied to voltage-polarity-independent resistive switching memory devices, *i.e.*, unipolar switching nonvolatile memory (USNM) devices, which require a high metal oxide surface area and high memory performance, *i.e.*, a high ON/OFF current ratio, a low OFF current, and memory stability. The ON/OFF current ratios of USNM devices prepared from LbL-assembled (PAA/OA-TiO_2 NP)$_n$ nanocomposite films increased to $\sim 10^9$ without high-temperature thermal treatment. Additionally, the OFF current was approximately 10^{-12} A at a reading voltage of 0.1 V. Previously reported approaches required thermal treatment at 400 °C.[33] Inorganic NP/polymer nanocomposites can be widely used in functional films/devices; therefore we believe that our approach can provide a basis for designing and exploiting high-performance nanocomposite films with the inherent functionalities and synergetic effects of water-soluble polymers and hydrophobic NPs.

2. Experimental section

Preparation of multilayers

The synthesis of OA-NPs (*i.e.*, OA-Ag, OA-Pt, OA-TiO_2, and OA-Fe_3O_4 NPs) dispersed in toluene is described in the detailed experimental section of the ESI.† Prior to the H/H LbL assembly, the negatively charged quartz or silicon substrates were prepared using an ammonia solution ($H_2O/NH_4OH/H_2O_2$ 5 : 1 : 1 v/v/v). The substrates were first dipped into the cationic poly(allylamine hydrochloride) (PAH) solution for 10 min, washed twice with water, and dried under a gentle air stream. The formed cationic substrates (PAH-coated substrates) were then dipped into another water-soluble polymer (*i.e.*, PAA, PVA, PEO, catalase, ferritin, and hemoglobin) solution, washed with water and dried with nitrogen. In the case of PDDA with cationic charges, anionic PAA was further deposited onto PAH-coated substrates, and then these substrates were dipped into the PDDA solution. After polymer adsorption, the water-soluble polymer-coated substrates were dipped into a hydrophobic OA-NP solution for 30 min, washed with toluene and dried in air. The substrates were then dipped into the water-soluble solution for another 30 min. These dipping and washing cycles were repeated until the desired number of layers had been obtained.

Analysis of the build-up of multilayers

Quantitative and qualitative analyses of the build-up of (OA-NP/water-soluble polymer)$_n$ multilayers were performed using UV-vis spectroscopy, quartz crystal microscopy (QCM), and Fourier transform infrared (FTIR) spectroscopy. The experimental details are described in the ESI.†

Fabrication of unipolar switching memory devices

The USNM devices based on the (PAA/OA-TiO_2 NP)$_n$ multilayer films were prepared as follows. First, the multilayer films were prepared on Pt-coated Si substrates (2 cm × 2 cm), followed by a drying process at 100 °C. Afterwards, Ag electrodes with a diameter of 100 μm were deposited onto the resultant multilayer films. To investigate the USNM behavior of the (PAA/OA-TiO_2 NP)$_n$ multilayered devices, the current–voltage (*I–V*) curves were collected using a semiconductor parametric analyzer (SPA, Agilent 4155B) in an air environment. The pulsed voltage duration dependence of the high- and low-current states was investigated using a semiconductor parametric analyzer (HP 4155A) and a pulse generator (Agilent 81104A).

3. Results and discussion

Various well-defined metal and metal oxide NPs stabilized by OA ligands (*i.e.*, OA-Ag, OA-Pt, OA-TiO_2, and OA-Fe_3O_4 NPs) prepared in toluene, and PAA in aqueous media, were used for the H/H LbL assembly (Fig. 1). First, to show that OA-TiO_2 NPs of diameter 10.5 ± 1.2 nm have high affinity toward PAA, which is a weak PE, PAA (at pH 3) was directly deposited on OA-TiO_2 NP-coated substrate. The resultant multilayer structure was cationic PAH-coated substrate/PAA/OA-TiO_2 NP/PAA. The amount of the residual OA ligand in the OA-TiO_2 NPs sandwiched between adjacent PAA layers was investigated as a function of

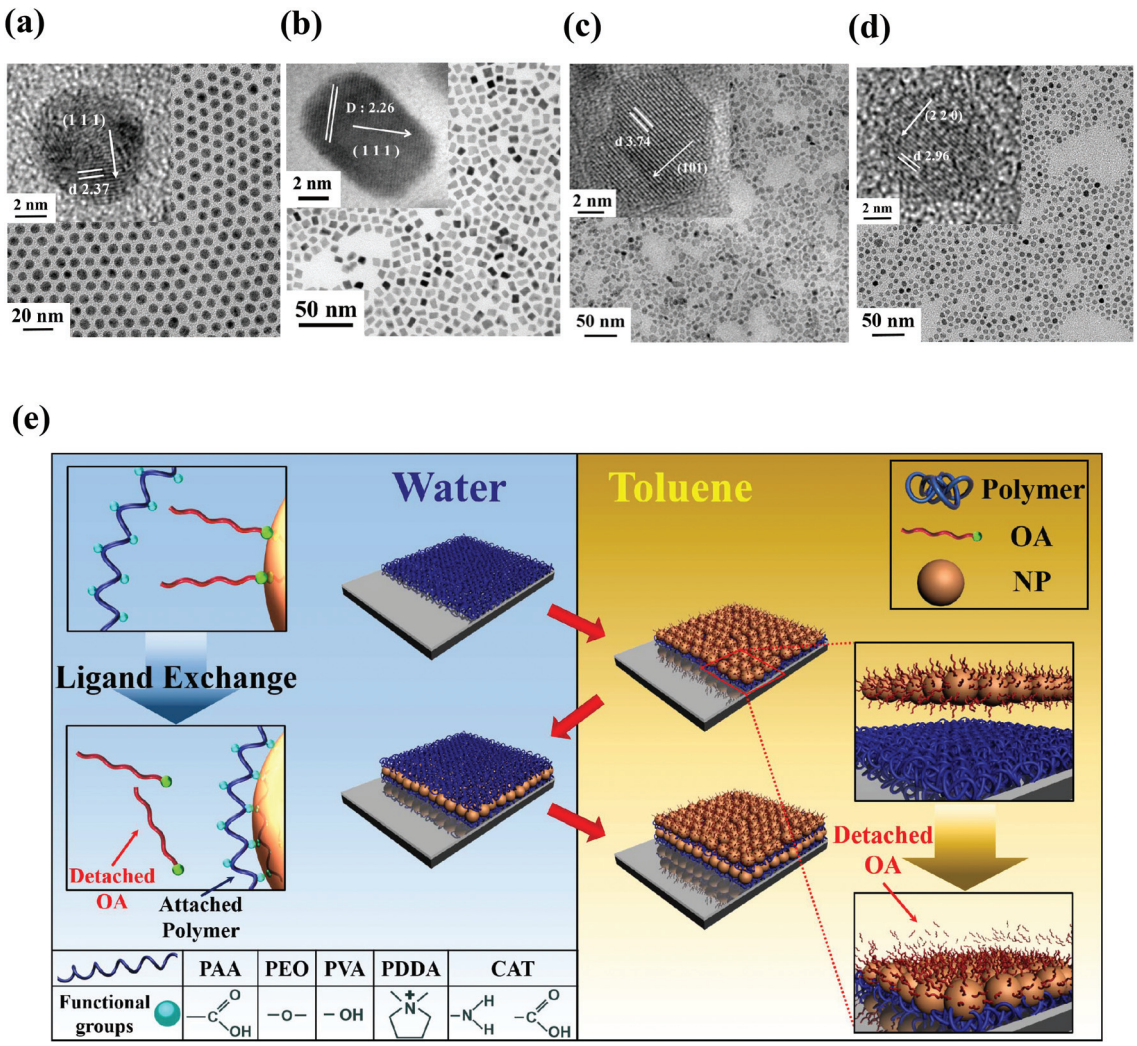

Fig. 1 High-resolution transmission electron microscopy images of (a) OA-Ag (diameter ~6.5 nm), (b) OA-Pt (~8 nm), (c) OA-TiO_2 (~10.5 nm), and (d) OA-Fe_3O_4 NPs (~6 nm); and (e) the schematic diagram of the preparation of (water-soluble polymer/OA-NP)$_n$ nanocomposite multilayers *via* a versatile amphiphilic LbL-assembly approach. Although the adsorbed OA-NP layers have a number of defects in their packing structure, the NP layer structure in (e) was depicted as an ideal packing structure for highlighting the densely coated OA-NPs.

the adsorption time of the outermost PAA layer using Fourier-transform infrared (FTIR) spectroscopy in advanced grazing angle specular reflectance (AGA) mode (Fig. 2a and ESI, Fig. S1†). Although the pristine OA ligands bear carboxylic acid (–COOH) moieties, these groups are bound to the metal oxide, *e.g.*, TiO_2, surfaces as carboxylate ions ($–COO^-$). The observed C–H stretching (2927 and 2855 cm^{-1}) and COO^- stretching (1553 and 1456 cm^{-1}) peaks therefore originate from long aliphatic chains, and from COO^- groups of the OA ligands bound to TiO_2 NPs, respectively.[28,30] The FTIR spectrum of PAA (at pH 3) also had clear absorption peaks for the COOH stretching vibration mode (1725 cm^{-1}) and a relatively weak absorption peak for the COO^- stretching mode (1553 and 1456 cm^{-1}). The COO^- stretching modes at 1553 and 1456 cm^{-1}, which arise from the OA ligands, therefore almost overlap with the peaks originating from PAA. When the adsorption time of the outermost PAA layer was increased from 10 min to 12 h, the intensities of the C–H stretching (2929 and 2855 cm^{-1}) peaks originating from the long aliphatic chains of the OA ligands gradually decreased. In contrast, the absorption peak (1725 cm^{-1}) associated with the COOH stretching vibration mode of PAA intensified slightly.[32,34] These results indicate that the OA ligands bound to the surfaces of the TiO_2 NPs were replaced by the –COOH groups of PAA.

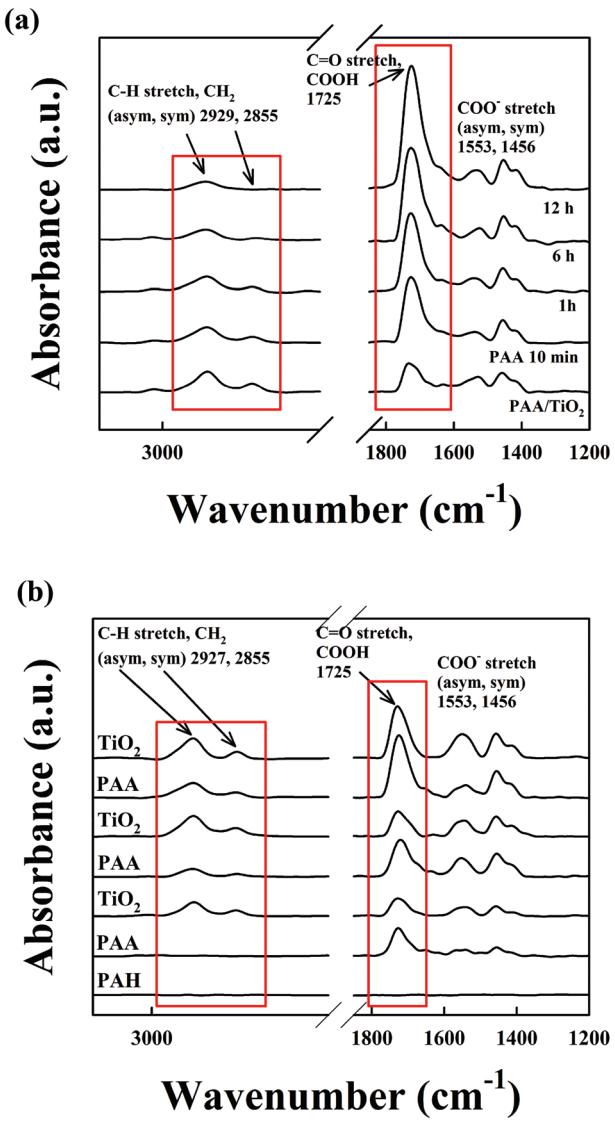

Fig. 2 Attenuated total reflectance-FTIR spectra of LbL-assembled films as a function of (a) deposition time of the PAA layer and (b) the layer number of $(PAA/OA\text{-}TiO_2)_n$ multilayers.

On the basis of this adsorption mechanism, we further investigated the changes in the two absorption peaks of the residual OA ligands and PAA at pH 3. PAA and OA-TiO_2 NPs were alternately deposited on a cationic substrate. The PAA and OA-TiO_2 NP adsorption times were fixed at 20 min. Fig. 2b shows that PAA adsorption on the substrate produced a strong absorption peak originating from the COOH stretching mode, at 1725 cm^{-1} (*i.e.*, a 0.5 bilayer). However, when the outermost layer was changed from PAA to OA-TiO_2 NPs, absorption peaks (2929 and 2855 cm^{-1}) indicating the presence of residual OA ligands on the surface of the outermost TiO_2 NP layer were observed, *i.e.*, single-bilayer films. The intensity of the absorption peak at 1725 cm^{-1} (assigned to the –COOH groups of PAA) decreased slightly because the residual –COOH moieties of PAA were bound to the metal oxide surface as carboxylate ion groups. Alternating deposition of PAA and OA-TiO_2 NPs resulted in inversely correlated changes in the peak intensities of the C–H stretching and COOH stretching vibration modes. Although the –COOH moieties of PAA are identical to those of the OA ligands in terms of binding sites, the observed ligand-exchange reaction implies that the PAA chains, which have numerous –COOH groups, act as multidentate ligands (or polymeric ligands), binding to Ti *via* one or two O atoms when they are adsorbed on the OA-TiO_2 NP surfaces. Based on these results, we conclude that PAA provides enhanced coordination interactions for the surface modification of the outermost TiO_2 NP layer, resulting in cooperative multiple binding instead of the OA ligand operating as a monodentate or bidentate ligand. This type of ligand-exchange LbL assembly (*i.e.*, H/H LbL assembly) is driven by the entropy increase[35] during adsorption.

Another notable feature is that the adsorbed amounts of OA-TiO_2 NPs and PAA can be easily controlled *via* the pH of the PAA solution. The amounts of adsorbed PAA and OA-TiO_2 NPs as a function of the PAA solution pH were determined quantitatively using a quartz-crystal microbalance (QCM). Fig. 3a shows that the alternating deposition of pH 3 PAA and OA-TiO_2 NPs resulted in mass change (Δm) $\approx$ 0.35 μg cm^{-2} (calculated from frequency change, $\Delta F \approx 20 \pm 3$ Hz) and 2.06 μg cm^{-2} ($\Delta F \approx 117 \pm 7$ Hz) per layer, respectively. The diameter and mass density of the TiO_2 NPs were about 10.5 nm and 3.78 g cm^{-3}, respectively, therefore the number density and three-dimensional packing density of the TiO_2 NPs in each TiO_2 NP layer were calculated to be approximately 8.99×10^{11} cm^{-2} (by QCM analysis) and 51.9% (or a two-dimensional packing density of ~77.8%), respectively. These values are

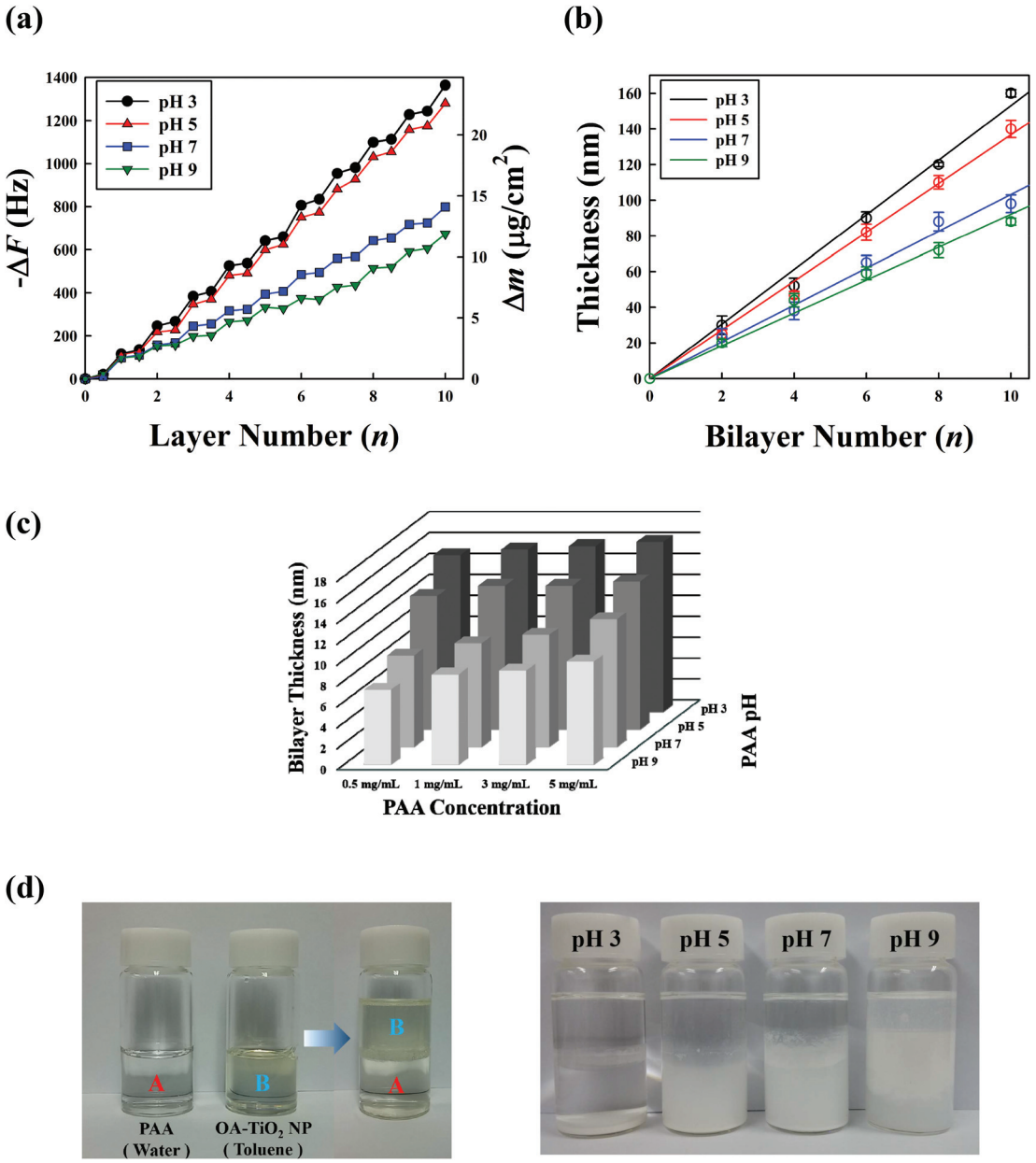

Fig. 3 (a) Dependence of the QCM frequency on the layer number of (PAA/OA-TiO_2 NP)$_n$ films at PAA pH values of 3, 5, 7, and 9. (b) Total film thicknesses of (pH 3 PAA/OA-TiO_2 NP)$_n$ multilayers measured from cross-sectional SEM images. (c) pH matrix showing the average thickness contributed by the PAA/OA-TiO_2 NP bilayer as a function of PAA solution concentration. (d) Phase transfer of OA-TiO_2 NPs from toluene to pH-controlled PAA solution. As the pH value increases from 9 to 3, the carboxylic acid groups of PAA were changed from highly ionized to neutralized states, and thus the hydrophobicity of PAA-stabilized TiO_2 NPs in water was increased. As a result, most of the PAA-stabilized TiO_2 NPs were precipitated at pH 3. Deposition times for pH 3 PAA and OA-TiO_2 NPs used in (a), (b), and (c) were fixed at 10 min. Solution concentrations of pH 3 PAA and OA-TiO_2 NPs used in (a)–(d) were 1 and 5 mg mL^{-1}, respectively.

close to the maximum packing density, corresponding to a random close-packed density of ~64% in a cubic volume of identical solid spheres. However, it has been reported that electrostatic repulsion among aqueous NPs with the same charges in the electrostatic LbL assembly considerably reduced the packing density of a NP layer (<30%).[36] As a result, the total film thicknesses of (pH 3, 1 mg mL^{-1} PAA/5 mg mL^{-1} OA-TiO_2 NPs)$_n$ multilayers measured based on cross-sectional scanning electron microscopy (SEM) images increased from approximately 30 to 160 nm when the bilayer number (n) was increased from 2 to 10 (Fig. 3b and ESI, Fig. S2†). However, when the pH of PAA was increased to 9, the adsorbed amounts of PAA (1 mg mL^{-1}) and OA-TiO_2 NPs (5 mg mL^{-1}) decreased to 0.113 μg cm^{-2} (ΔF = 7 ± 2 Hz) and 1.08 μg cm^{-2} (ΔF = 61 ± 9 Hz) per layer, respectively. In this case, the number density and three-dimensional packing density (per layer) of TiO_2 NPs

adsorbed on the pH 9 PAA were calculated to be approximately 4.72×10^{11} cm^{-2} (by QCM analysis) and 27.1%, respectively. The total thickness of (pH 9 PAA/OA-TiO_2 NP)$_{10}$ multilayers was approximately 88 nm. This thickness change was also influenced by the PAA solution concentration. Fig. 3c shows the average incremental thickness of the PAA/OA-TiO_2 NP bilayer as functions of the PAA solution pH and concentration. When the pH and concentration of the PAA solution were changed from pH 9 and 0.5 mg mL^{-1} to pH 3 and 5 mg mL^{-1}, respectively, the average thickness of the PAA/OA-TiO_2 NP bilayer increased from approximately 6 to 16 nm. In our system, the bilayer thickness strongly depended on the PAA solution pH. As previously mentioned, this pH-dependent adsorption behavior of OA-TiO_2 NPs is mainly caused by the charge state of PAA enabling it to act as a multidentate ligand. When the solution pH is increased from 3 to 9, a large amount of the uncharged –COOH groups of PAA is converted into negatively charged COO^- groups (pK_a of PAA ≈4.5). This conversion increases the electrostatic repulsion among the COO^- groups of PAA, resulting in a low PAA loading.[32] In line with the PAA adsorption behavior, the amount of OA-TiO_2 NPs adsorbed on the pH 9 PAA layer was lower than that on the pH 3 PAA layer. We cannot exclude the possibility that a change in the surface charge of the bare TiO_2 NPs at pH 9 partly contributes to the adsorption behavior of the OA-TiO_2 NPs. Organic-ligand-free TiO_2 NPs dispersed in aqueous solution have been reported to be positively charged below, and negatively charged above, pH 6.[37,38] In the case of highly ionized PAA deposited on an OA-TiO_2 NP layer at pH 9, electrostatic repulsion between PAA and the bare surfaces of the TiO_2 NPs could therefore occur during *in situ* ligand exchange between the PAA and OA ligands bound to the TiO_2 NP surfaces. This exchange could decrease the amount of adsorbed PAA, followed by a decrease in the loaded amount of OA-TiO_2 NPs. Although the pH of the PAA solution greatly affects the amount of adsorbed OA-TiO_2 NPs, the resultant (PAA/OA-TiO_2 NP)$_n$ films prepared in the pH range of 3–9 had highly uniform and homogeneous surface structures, despite their different hydrophobic/hydrophilic properties (see ESI, Fig. S2†). We confirmed that a variety of inorganic NPs (*i.e.*, OA-Ag, OA-Pt NP, and OA-Fe_3O_4 NPs) could be LbL assembled with PAA, and showed pH-dependent adsorption behaviors

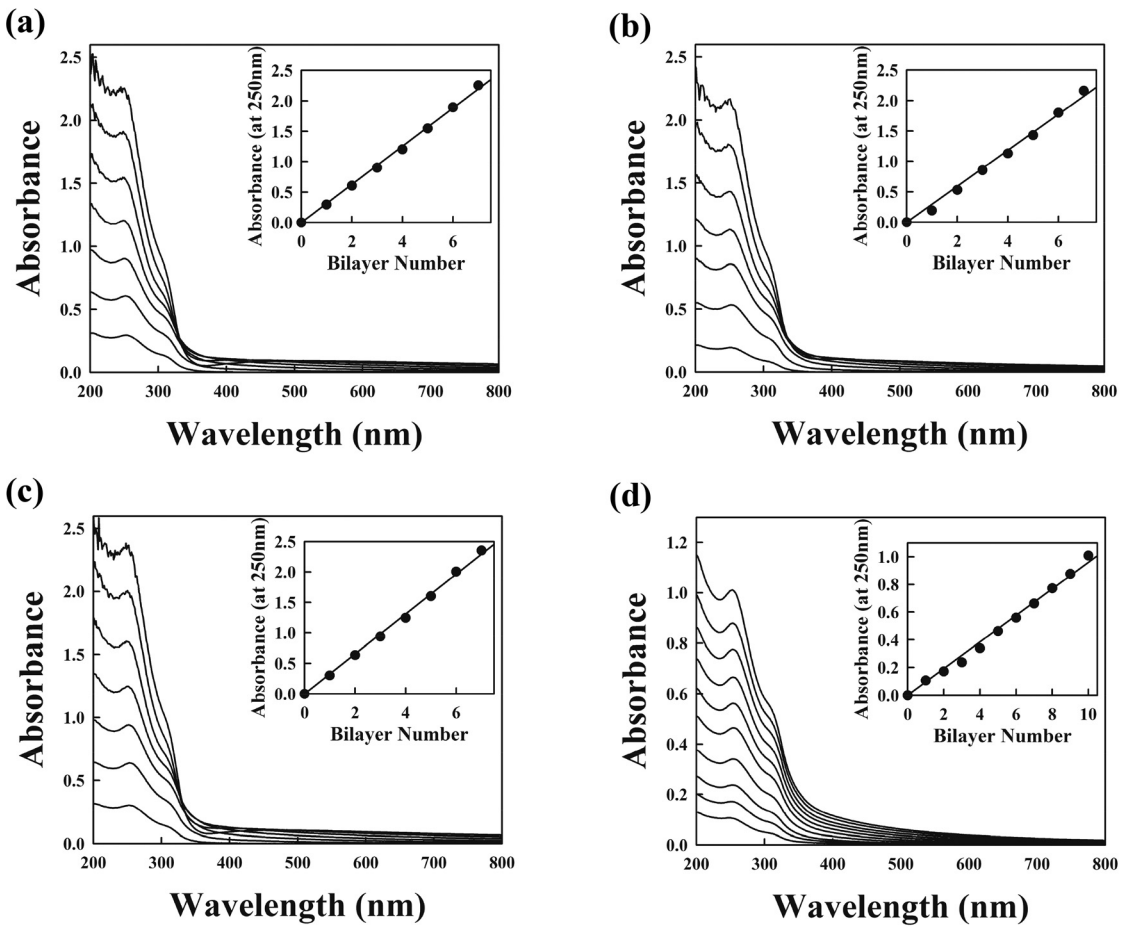

Fig. 4 UV-vis spectra of (a) (PVA/OA-TiO_2 NP)$_n$, (b) (PEO/OA-TiO_2 NP)$_n$, (c) (PDDA/OA-TiO_2 NP)$_n$, and (d) (CAT pH 3/OA-TiO_2 NP)$_n$ multilayers as a function of bilayer number (n). The insets show the UV-vis absorbance of (water-soluble polymer/hydrophobic NP)$_n$ multilayers as a function of n.

similar to that of the (PAA/OA-TiO_2 NP)$_n$ multilayers (see ESI, Fig. S3†).

The H/H LbL assembly was further investigated by performing phase transfer of the TiO_2 NPs from toluene to an aqueous medium by mixing an OA-TiO_2 NP solution with a pH-controlled PAA solution. After the OA-TiO_2 NPs and PAA solution had been mixed for 2 h, most of the TiO_2 NPs had been precipitated in the PAA aqueous solution (at pH 3, 5, and 7) or were dispersed at the interface between the toluene and aqueous solution (at pH 9) (Fig. 3d). These phenomena presumably occur because the affinity between PAA and the OA-TiO_2 NPs is insufficient to overcome the difference between the polarities of the nonpolar solvent for the OA-TiO_2 NPs and the PAA aqueous medium. That is, residual OA ligands still remain onto the surface of TiO_2 NPs even after a sufficient adsorption time for the ligand exchange reaction between PAA and OA, which decreases the hydrophilicity of the phase-transferred PAA-TiO_2 NPs. Furthermore, with decreasing the solution pH value from 9 to 3, the carboxylate ion ($-COO^-$) groups of PAA ligands onto TiO_2 NPs were fully converted into the non-ionized carboxylic acid (–COOH) groups, and resultantly the increased hydrophobicity of PAA-TiO_2 NPs (at pH 3) were rapidly precipitated.

Although the direct LbL assembly of these phase-transferred TiO_2 NPs (*i.e.*, anionic PAA-coated TiO_2 NPs) with cationic PEs for the preparation of nanocomposite films is difficult due to the poor dispersion of PAA-TiO_2 NPs in water, our approach shows that a variety of OA-NPs can be easily and directly incorporated into nanocomposite films *via* weak PEs, despite the relatively low affinity between PAA and the inorganic NP surfaces.

On the basis of these results, we investigated the LbL assemblies of OA-TiO_2 NPs with PVA, PDDA, PEO, and CAT using the same adsorption time and solution concentration as that used for the assembly of PAA/OA-TiO_2 NP nanocomposite multilayers. Fig. 4 shows that the UV-vis absorbance per bilayer of (PVA/OA-TiO_2 NP)$_n$, (PEO/OA-TiO_2 NP)$_n$, (PDDA/OA-TiO_2 NP)$_n$, and (CAT pH 3/OA-TiO_2 NP)$_n$ multilayers increased regularly with the increasing bilayer number, *i.e.*, OA ligands loosely bound to the OA-TiO_2 NP surfaces were easily replaced with various multidentate groups such as the hydroxyl groups of PVA, ether groups of PEO, tertiary

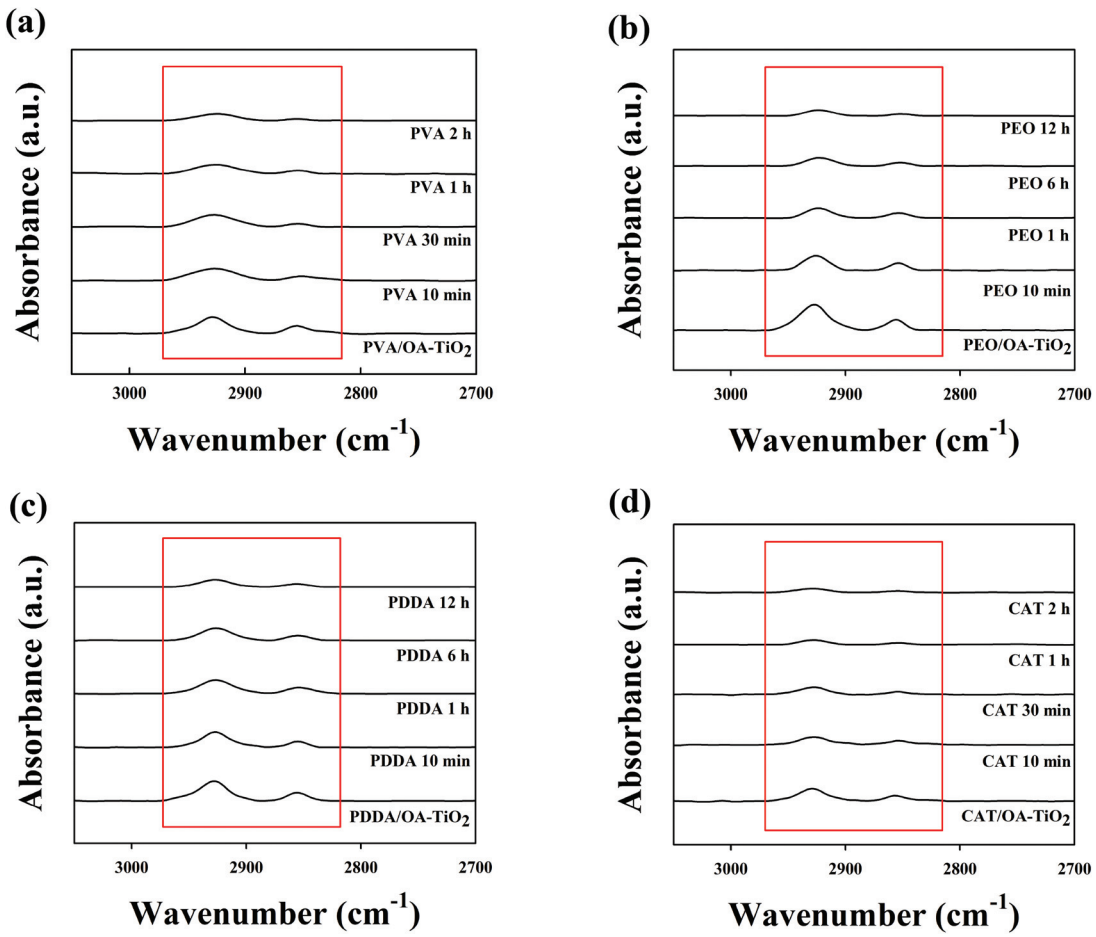

Fig. 5 AGA-FTIR spectra of LbL-assembled films as a function of deposition time of (a) PVA, (b) PEO, (c) PDDA, and (d) CAT layers adsorbed on OA-TiO_2 NP-coated substrates. Intensities of the observed C–H stretching (2855, 2927 cm^{-1}) peaks originating from the long aliphatic chains of the OA ligands bound to TiO_2 NPs gradually decreased with the increasing polymer deposition time.

ammonium groups of PDDA, or the amino acid groups of biomaterials, *i.e.*, CAT, ferritin, and hemoglobin (Fig. 5 and ESI, Fig. S4†). Additionally, it was confirmed that these polymers could be robustly deposited onto the OA-TiO_2 NP-coated substrates without inducing the detachment of OA-TiO_2 NPs from the substrates (see ESI, Fig. S5†). Furthermore, these results strongly suggest that our approach can be extended to a variety of biocompatible nanocomposites, overcoming the problems associated with different hydrophobic/hydrophilic properties without the need for any additional chemical modification.

Despite the use of water-soluble polymers, our approach can be effectively applied to the production of memory devices (specifically USNM devices with a switching procedure independent of the polarity of the applied voltage) with high memory performances. As previously mentioned, our group reported that various OA-NPs could be LbL assembled with

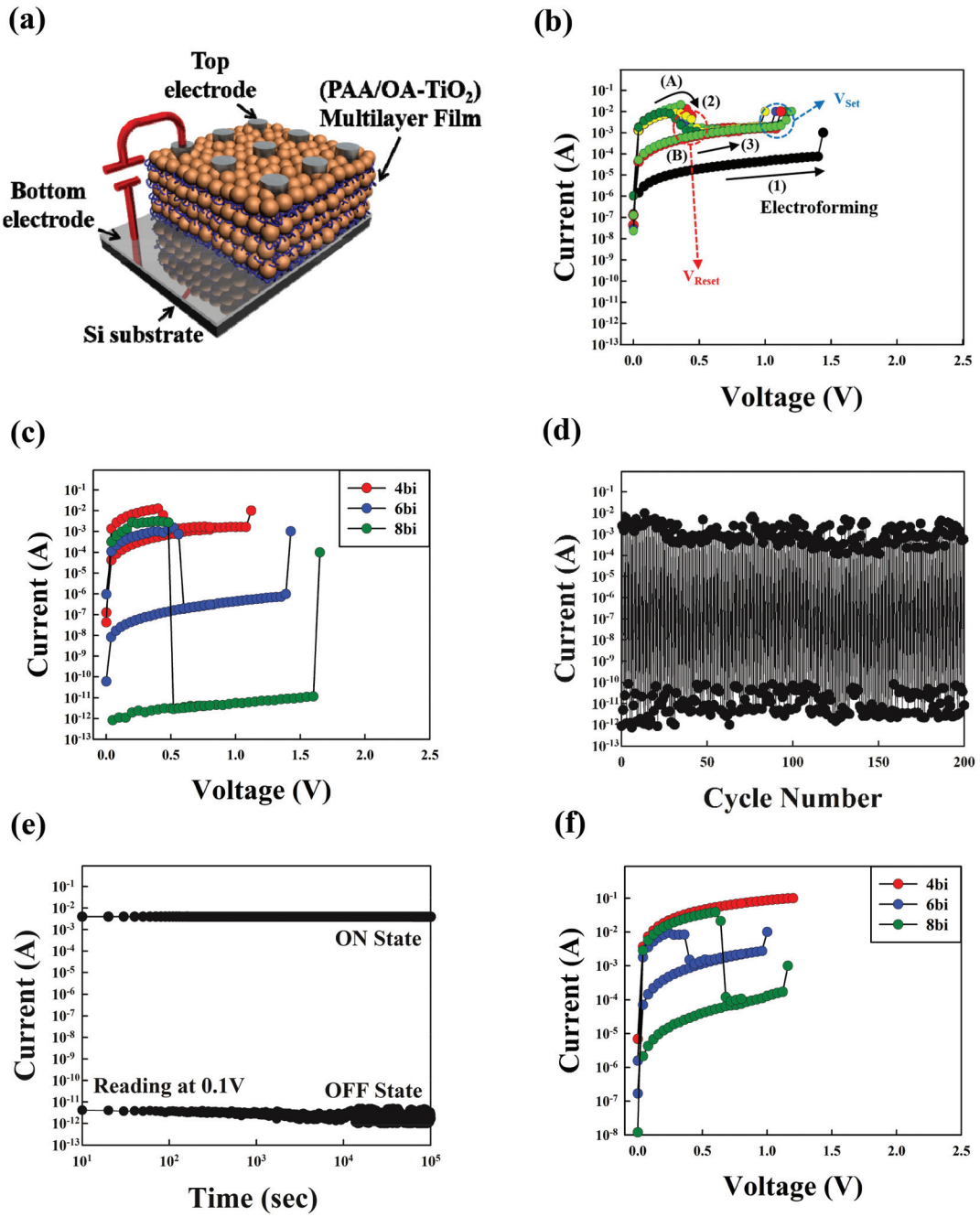

Fig. 6 Schematic diagram of the USNM device based on (PAA/OA-TiO_2 NP)$_4$ multilayers; (b) *I*–*V* curves of the (PAA/OA-TiO_2 NP)$_n$ multilayer device for repeated switching cycles after the initial electroforming process; (c) *I*–*V* curves of (PAA/OA-TiO_2 NP)$_n$ multilayer devices with the increasing bilayer number (*n*) from 4 to 8; (d) retention times and (e) cycling tests for the (PSS/OA-TiO_2 NP)$_8$ multilayer device; and (f) *I*–*V* curves of (PSS/OA-TiO_2 NP)$_n$ multilayer devices with increasing *n* from 4 to 8.

strong PEs containing SO_3^- groups and that the adsorbed amounts could be increased by the addition of ionic salts such as NaCl to the strong-PE deposition solution.[28] However, our previous approach was not suitable for USNM devices, which require a low leakage current level and a high ON/OFF current ratio, because of the polyanion doping effect of the strong sulfonic acid groups[39] and the possible presence of residual ionic salts in the nanocomposite films. Fig. 6a shows a USNM device composed of (pH 3 PAA/OA-TiO_2 NP)$_n$ multilayer films deposited on bottom-Pt-electrode-coated Si substrates, with top Ag electrodes of diameter 100 μm, deposited on the multilayer films. These devices were dried at 120 °C in air to completely remove the residual water molecules in the PAA layers. Electrical measurements were performed on the USNM cells at an applied voltage pulse of width 1 μs in air. During the first sweep of the applied positive voltage, the (PAA/OA-TiO_2 NP)$_4$ device showed a rapid increase in current at approximately 1.4 V (Fig. 6b). This electroforming of limited current compliance up to 1 mA initially formed a conductive path in the nanocomposite multilayers.[40] The high-current state (*i.e.*, the ON state) formed after the electroforming process returned to the low-current state, with an abrupt decrease in the current, at approximately 0.4–0.5 V (*i.e.*, the RESET voltage, V_{RESET} in region A) during the second voltage sweep from 0 to 0.8 V (Fig. 6b). When the applied voltage was increased again (*i.e.*, region B), the USNM device with a low-current state (*i.e.*, the OFF state) showed a rapid current increase at approximately 1.0–1.1 V (*i.e.*, the SET voltage, V_{SET}) and a resultant ON/OFF current ratio of $\sim10^2$. This unipolar switching behavior is caused by the formation and disruption of conducting filamentary paths in the oxide NP layers.[41] This is because the presence of oxygen-deficient states (*i.e.*, Ti^{3+}) in the TiO_2 NPs enables the PAA/OA-TiO_2 NP nanocomposite film to act like an n-type dopant, transforming the insulating nanocomposite into an electrically active film. The reversible formation (*i.e.*, the ON state as the high-current state) and disruption (*i.e.*, the OFF state as the low-current state) of a conducting filamentary path in the OA-TiO_2 NP layers under an applied voltage are caused by the voltage-induced partial dielectric breakdown and thermal breakdown, respectively, at higher voltages. In our system, the Ti $2p_{3/2}$ X ray-photoelectron spectroscopy peaks were resolved into two spin–orbit components assigned to Ti^{3+} (457.9 eV) and Ti^{4+} (458.4 eV) (see ESI, Fig. S6†).[42] The presence of the Ti^{3+} peak indicates the generation of oxygen vacancies in the films. The Ti^{3+}/Ti^{4+} ratio was approximately 0.23. These localized conductive paths were confirmed by the local current images obtained using current-sensing atomic force microscopy (see ESI, Fig. S7†).

The complete disruption of the conductive filamentary path in the OFF state with the increasing bilayer number (*i.e.*, total film thickness) of the (PAA/OA-TiO_2 NP)$_n$ films can be reasonably assumed to substantially decrease the leakage current level and thus increase the ON/OFF current ratio. We confirmed this assumption by investigating the nonvolatile memory performances of USNM devices with the increasing bilayer number (or total film thickness) of (PAA/OA-TiO_2 NP)$_n$ multilayers from 4 (64 nm) to 8 (128 nm). Fig. 6c shows that V_{SET} of the (PAA/TiO_2 NP)$_n$ multilayers increased slightly, from approximately 1.1 to 1.6 V, because of the increased film thickness. In contrast, the ON/OFF current ratio of the (PAA/OA-TiO_2 NP)$_n$ devices increased significantly, from $\sim10^2$ (OFF current of $\sim10^{-4}$ A) to $\sim10^9$ (OFF current of $\sim10^{-12}$ A), at a reading voltage of 0.1 V. Notably, nanocomposite film devices prepared using a vacuum deposition method, simple solution blending, or electrostatic LbL assembly generally have an ON/OFF current ratio of approximately 10^3 to 10^5.[33,43,44]

Cycling and retention time tests were also performed on a (PAA/OA-TiO_2 NP)$_8$ multilayer device to determine the memory stability in the ON and OFF states at a reading voltage of 0.1 V (Fig. 6d and e). The ON and OFF states were maintained during repeated cycling for a test period of 10^5 s, showing good electric stability. Kozicki *et al.* reported that solid electrolytes sandwiched between an Ag electrode and an inert electrode induce resistive switching as a result of an electrochemical redox reaction, based on the high mobility of Ag ions.[45] Electrochemically active Ag electrodes were used as the top electrodes in our system, but similar switching behaviors were also observed using electrochemically inactive electrodes such as Au, W, and Pt as the top electrodes (see ESI, Fig. S8†). In contrast, (PSS/OA-TiO_2 NP)$_n$ devices prepared by a strong-PE-induced amphiphilic LbL assembly gave low memory performances, with relatively high leakage current levels (*i.e.*, an ON/OFF current ratio of $\sim10^3$, and an OFF current of $\sim10^{-5}$ for a device with eight bilayers), compared to those of (PAA/OA-TiO_2 NP)$_n$ multilayer devices with the same film thicknesses (Fig. 6f). The average thickness (approximately 16 nm) of the PSS/OA-TiO_2 NP bilayer was determined by addition of 0.2 M NaCl to the PSS solution. These results imply that the type of inserted polymer substantially influences the electrical performance of the nanocomposite device. Our approach and findings will enable the effective use of the specific advantages of water-soluble polymers and hydrophobic NPs.

4. Conclusions

We showed that a variety of water-soluble polymers ranging from weak PEs to uncharged polymers could be directly LbL assembled with hydrophobic NPs (*i.e.*, OA-stabilized metal or metal oxide NPs) in nonpolar solvents *via* a ligand-exchange reaction between OA ligands loosely bound to the NP surfaces and the hydrophilic multidentate binding groups of water-soluble polymers. When a weak PE such as PAA was used, the OA-NP loading could be adjusted *via* the pH and/or concentration of the PAA solution. These results imply that well-defined hydrophobic NPs can be easily incorporated into a variety of water-soluble polymers without additional surface modification or encapsulation. Furthermore, the adsorption behavior of hydrophobic NPs can be controlled based on various assembly conditions for the adsorption of water-soluble polymers on the substrate. Our approach can induce

almost perfect combination of hydrophobic NPs in nonpolar media and water-soluble materials in aqueous media without segregation or agglomeration. Furthermore, our approach can be used to fabricate high-performance nonvolatile memory devices. USNM devices composed of $(PAA/OA\text{-}TiO_2\ NP)_8$ showed excellent unipolar switching memory performances with a high ON/OFF current ratio of $\sim 10^9$ and an extremely low OFF current of $\sim 10^{-12}$ A. Given that the end-use and performance of polymer/inorganic NP nanocomposite films strongly depend on the functionalities, structures, surface polarities, and loading amounts of the respective components in the films, we believe that our approach can provide a basis for developing novel functional films and for enhancing performances in various potential applications such as in data-storage, electrochemical, energy-storage, and optical devices.

Acknowledgements

This work was supported by the National Research Foundation of Korea (NRF) grant funded by the Ministry of Science, ICT & Future Planning (MSIP) (2015R1A2A1A01004354).

References

1 H. Zou, S. Wu and J. Shen, *Chem. Rev.*, 2008, **108**, 3893–3957.
2 C. J. Mable, R. R. Gibson, S. Prevost, B. E. Mckenzie, O. O. Mykhaylyk and S. P. Armes, *J. Am. Chem. Soc.*, 2015, **137**, 16098–16108.
3 S. K. Cha, J. H. Mun, T. Chang, S. Y. Kim, J. Y. Kim, H. M. Jin, J. Y. Lee, J. Shin, K. H. Kim and S. O. Kim, *ACS Nano*, 2015, **9**, 5536–5543.
4 A. K. Boal, F. Ilhan, J. E. DeRouchey, T. Thurn-Albrecht, T. P. Russell and V. M. Rotello, *Nature*, 2000, **404**, 746–748.
5 O. Uzun, B. L. Frankamp, A. Sanyal and V. M. Rotello, *Chem. Mater.*, 2006, **18**, 5404–5409.
6 J. Pang, S. Xiong, F. Jaeckel, Z. Sun, D. Dunphy and C. J. Brinker, *J. Am. Chem. Soc.*, 2008, **130**, 3284–3285.
7 H. Ejima, J. J. Richardson, K. Liang, J. P. Best, M. P. van Koeverden, G. K. Such, J. Cui and F. Caruso, *Science*, 2013, **341**, 154–157.
8 R. K. Iler, *J. Colloid Interface Sci.*, 1966, **21**, 569–594.
9 G. Decher, *Science*, 1997, **277**, 1232–1237.
10 F. Caruso, R. A. Caruso and H. Möhwald, *Science*, 1998, **282**, 1111–1114.
11 T. Cassagneau, T. E. Mallouk and J. H. Fendler, *J. Am. Chem. Soc.*, 1998, **120**, 7848–7859.
12 T. Ogoshi, S. Takashima and T. Yamagishi, *J. Am. Chem. Soc.*, 2015, **137**, 10962–10964.
13 A. J. Gormley, R. Chandrawati, A. J. Christofferson, C. Loynachan, C. Jumeaux, A. Artzy-Schnirman, D. Aili, I. Yarovsky and M. M. Stevens, *Chem. Mater.*, 2015, **27**, 5820–5824.
14 Y. Kim, J. Zhu, B. Yeom, M. D. Prima, X. Su, J.-G. Kim, S. J. Yoo, C. Uher and N. A. Kotov, *Nature*, 2013, **500**, 59–64.
15 A. Vaterrodt, B. Thallinger, K. Daumann, D. Koch, G. M. Guebitz and M. Ulbricht, *Langmuir*, 2016, **32**, 1347–1359.
16 Y. Kim, K. Y. Lee, S. K. Hwang, C. Park, S.-W. Kim and J. Cho, *Adv. Funct. Mater.*, 2014, **24**, 6262–6269.
17 Y. Ko, D. Shin, B. Koo, S. W. Lee, W.-S. Yoon and J. Cho, *Nano Energy*, 2015, **12**, 612–625.
18 K. Yin, Z. Zhou, D. E. Schuele, M. Wolak, L. Zhu and E. Baer, *ACS. Appl. Mater. Interfaces*, 2016, **8**, 13555–13566.
19 B. Lee, Y. Kim, S. Lee, Y. S. Kim, D. Wang and J. Cho, *Angew. Chem., Int. Ed.*, 2010, **49**, 359–363.
20 D. Kim, Y. Kim and J. Cho, *Chem. Mater.*, 2013, **25**, 3834–3843.
21 M. Jiang, D. Zhu, J. Cai, H. Zhang and X. Zhao, *J. Phys. Chem. C*, 2014, **118**, 14371–14378.
22 Y. Kim, C. Lee, I. Shim, D. Wang and J. Cho, *Adv. Mater.*, 2010, **22**, 5140–5144.
23 P. Y. Keng, B. Y. Kim, I.-B. Shim, R. Sahoo, P. E. Veneman, N. R. Armstrong, H. Yoo, J. E. Pemberton, M. M. Bull, J. J. Griebel, E. L. Ratcliff, K. G. Nebesny and J. Pyun, *ACS Nano*, 2009, **3**, 3143–3157.
24 W. C. W. Chan and S. Nie, *Science*, 1998, **281**, 2016–2018.
25 J. Park, K. An, Y. Hwang, J.-E. Park, H.-J. Noh, J.-Y. Kim, J.-H. Park, N.-M. Hwang and T. Hyeon, *Nat. Mater.*, 2004, **3**, 891–895.
26 M. K. Corbierre, N. S. Cameron, M. Sutton, S. G. J. Mochrie, L. B. Lurio, A. Rühm and R. B. Lennox, *J. Am. Chem. Soc.*, 2001, **123**, 10411–10412.
27 D. Kim, S. Cheong, Y. G. Ahn, S. W. Ryu, J.-K. Kim and J. Cho, *Nanoscale*, 2016, **8**, 7000–7016.
28 M. Park, Y. Kim, Y. Ko, S. Cheong, S. W. Ryu and J. Cho, *J. Am. Chem. Soc.*, 2014, **136**, 17213–17223.
29 K. Nakamoto, *Infrared and Raman Spectra of Inorganic and Coordination Compounds*, A John Wiley & Sons, Inc., New Jersey, 2008.
30 S. Sun, *Adv. Mater.*, 2006, **18**, 393–403.
31 I. V. Chernyshova, S. Ponnurangam and P. Somasundaran, *Langmuir*, 2011, **27**, 10007–10018.
32 J. Choi and M. F. Rubner, *Macromolecules*, 2005, **38**, 116–124.
33 C. Lee, I. Kim, W. Choi, H. Shin and J. Cho, *Langmuir*, 2009, **25**, 11276–11281.
34 J. Cho, J. Hong, K. Char and F. Caruso, *J. Am. Chem. Soc.*, 2006, **128**, 9935–9942.
35 W. Lin, K. Fritz, G. Guerin, G. R. Bardajee, S. Hinds, V. Sukhovatkin, E. H. Sargent, G. D. Scholes and M. A. Winnik, *Langmuir*, 2008, **24**, 8215–8219.
36 J. Schmitt, G. Decher, W. J. Dressick, S. L. Brandow, R. E. Geer, R. Shashidhar and J. M. Calvert, *Adv. Mater.*, 1997, **9**, 61–65.
37 T. H. Tran, A. Y. Nosaka and Y. Nosaka, *J. Phys. Chem. B*, 2006, **110**, 25525–25531.
38 D. Lee, D. Omolade, R. E. Cohen and M. F. Rubner, *Chem. Mater.*, 2007, **19**, 1427–1433.

39 O. Onitsuka, A. C. Fou, M. Ferreira, B. R. Hsieh and M. F. Rubner, *J. Appl. Phys.*, 1996, **80**, 4067–4071.
40 R. Waser and M. Aono, *Nat. Mater.*, 2007, **6**, 833–840.
41 K. Szot, W. Speier, G. Bihlmayer and R. Waser, *Nat. Mater.*, 2006, **5**, 312–320.
42 *NIST X-ray Photoelectron Spectroscopy Database, Version 4.1*, National Institute of Standards and Technology, Gaithersburg, 2012; http://srdata.nist.gov/xps/.
43 W. Elsawy, M. Son, M. I. Kim, Y. Ji, T.-W. Kim, H. C. Ko, A. Elbarbary, M.-H. Ham and J.-S. Lee, *ACS Macro Lett.*, 2015, **4**, 322–326.
44 C. Schindler, S. C. P. Thermadam, R. Waser and M. N. Kozicki, *IEEE Trans. Electron Devices*, 2007, **54**, 2762–2768.
45 M. N. Kozicki, M. Yun, L. Hilt and A. Singh, *Applications of Programmable Resistance Changes in Metal-Doped Chalcogenides*, The Electrochemical Society, New Jersey, 1999.